

# Comparative Study of the Thermal Stabilities of the Experimentally Known High-Valent Fe(IV) Compounds Fe(1-norbornyl)<sub>4</sub> and Fe(cyclohexyl)<sub>4</sub>

Huidong Li,<sup>a,b</sup> Linshen Wang,<sup>a</sup> Yuchen Hu,<sup>a</sup> Ze Zhang,<sup>a</sup> Di Wan, Qunchao Fan,<sup>a\*</sup> R. Bruce King,<sup>b\*</sup> and Henry F. Schaefer<sup>b</sup>

<sup>a</sup> School of Science, Key Laboratory of High Performance Scientific Computation, Xihua University, Chengdu, China 610039

<sup>b</sup> Department of Chemistry and Center for Computational Chemistry, University of Georgia, Athens, Georgia 30602, USA

[rbking@chem.uga.edu](mailto:rbking@chem.uga.edu); [fanqunchao@sina.com](mailto:fanqunchao@sina.com)

## Abstract

The high stability of the experimentally known homoleptic 1-norbornyl derivative (nor)<sub>4</sub>Fe of iron in the unusual +4 oxidation state is a consequence of the high reaction barriers of the singlet or triplet potential surfaces constrained by the global dispersion attraction and the large steric demands of the norbornyl groups. The much more limited stability of the corresponding cyclohexyl derivative (cx)<sub>4</sub>Fe may result from the conical intersection between the singlet potential surface and the quintet spin potential surface arising from the weaker dispersion attraction and the reduced steric effect of the cyclohexyl groups relative to the 1-norbornyl groups. In contrast, the high stability of the likewise experimentally known (cx)<sub>4</sub>M (M = Ru or Os) structures results from the larger ligand field splitting ( $\Delta$ ) of the d-orbital energies for the second and third row transition metals ruthenium and osmium relative to that of the first row transition metal iron. The cyclohexyl derivative (cx)<sub>4</sub>Fe is predicted to be reactive towards carbon monoxide to insert CO into up to two Fe–C bonds. However, the dispersion effect as well as the much larger size of the 1-norbornyl substituents prevents similar reactivity of (nor)<sub>4</sub>Fe with carbon monoxide.

## 1. Introduction

Iron derivatives in the unusual +4 formal oxidation state are of interest as agents for activating C-H bonds to introduce halogen or oxygenic substituents.<sup>1,2</sup> In this connection many spectroscopic and synthetic studies focus on Fe(IV) heteroleptic complexes. However, relatively few homoleptic Fe(IV) species are known and the few known such species have received relatively little attention.<sup>3,4,5,6,7,8</sup> The species (cx)<sub>4</sub>Fe (cx = cyclohexyl)<sup>2,7</sup> and (nor)<sub>4</sub>Fe (nor = 1-norbornyl)<sup>3,5</sup> are two important representative compounds with the four alkyl ligands coordinated to the central Fe(IV) atom in a nearly ideal tetrahedral environment (Figure 1). Dispersion effects have been shown to be significant in stabilizing such species. However, the thermal stabilities of these two R<sub>4</sub>Fe structures were observed to be totally different. Thus (cx)<sub>4</sub>Fe is stable only below -20 °C,<sup>2,3</sup> whereas (nor)<sub>4</sub>Fe remains stable at 23 °C.<sup>7</sup> The mechanism for the thermal decomposition of these two R<sub>4</sub>Fe complexes remains fully unknown although the attractive dispersion effect has been suggested as a factor determining their relative stabilities. Thus the dispersion force imposed by the much larger 1-norbornyl groups in the (nor)<sub>4</sub>Fe structure is considered to be larger than that for the cyclohexyl groups in the (cx)<sub>4</sub>Fe structure.<sup>2,3</sup> However, theoretical studies on how the dispersion effect can lead to such different thermal stabilities are still very limited. The cyclohexyl ligands in (cx)<sub>4</sub>Fe are much more amenable to reductive coupling, homolytic bond cleavage, and  $\beta$ - and  $\gamma$ -hydride elimination relative to the 1-norbornyl ligands in (nor)<sub>4</sub>Fe. However, the strong dispersion attraction and high ring constraint of the 1-norbornyl ligands in (nor)<sub>4</sub>Fe make  $\beta$ - and  $\gamma$ -hydride elimination unlikely. Furthermore, the crowded environment caused by the tightly interlocked 1-norbornyl fragments hinders the penetration of small molecules to interact with the Fe-C bonds. Such factors lead to reduced chemical reactivity of (nor)<sub>4</sub>Fe relative to (cx)<sub>4</sub>Fe.<sup>3</sup>



**Figure 1.** The experimentally known Fe(IV) Compounds Fe(1-norbornyl)<sub>4</sub><sup>2,3</sup> and Fe(cyclohexyl)<sub>4</sub>.<sup>5,7</sup>

In sterically crowded molecules with large hydrocarbon substituents, steric repulsion and attractive dispersion forces are substantial enough to influence their

physical and chemical properties. London dispersion forces, which are always present, become significant enough to influence the stability, structure, and reactivity of inorganic and organometallic derivatives bearing sterically large groups. The London dispersion forces in such molecules with bulky organic groups are sufficient to hold the molecule together.<sup>9,10,11,12,13,14,15</sup> In addition, for compounds containing high-valent metal centers, the strong Coulombic interactions resulting from the high charge density on the metal atoms can also significantly affect their stabilities. The competition between dispersion and electrostatic interactions may simultaneously determine the chemical and physical properties of the inorganic and organometallic derivatives.

The 1-norbornyl and cyclohexyl groups both are reasonably strong field ligands also providing significant attractive London dispersion forces and Coulombic interactions to stabilize abnormally high formal metal oxidation states in alkyl derivatives. However, the dispersion effect and Coulombic interactions are not sufficient to account for the extreme stabilities of the isostructural homologues (cx)<sub>4</sub>Ru and (cx)<sub>4</sub>Os having metal-carbon bonding distances similar to the much less stable (cx)<sub>4</sub>Fe structure.<sup>16</sup> The relative instability of the (cx)<sub>4</sub>Fe structure is suggested to relate to the equatorial disposition of the central iron atom on the cyclohexyl ring causing steric repulsion. This kind of conformational change could be precluded by the attractive dispersion and Coulombic interactions both in (nor)<sub>4</sub>Fe and (cx)<sub>4</sub>Fe. In order to provide a more detailed understanding of the widely different stabilities of (nor)<sub>4</sub>Fe and (cx)<sub>4</sub>Fe we have now undertaken a detailed theoretical study reported here.

## 2. Theoretical Methods

Dispersion effects are found to be important in structures containing sterically demanding groups<sup>6,13,17</sup> Thus computational studies have shown that some molecules can be stabilized significantly by dispersion effects.<sup>10,16</sup> The B3PW91-D3 method<sup>18,19</sup> with Grimme's D3 dispersion scheme<sup>20,21</sup> and the hybrid *meta*-GGA DFT method  $\square$ B97xD functional<sup>22</sup> including empirical dispersion contributions were used with the Gaussian 09 program<sup>23</sup> to optimize the geometries of all structures in the present paper. The reduced density gradients (RDG)<sup>24</sup> indicating the noncovalent weak interactions implemented in Multiwfn<sup>25</sup> were used to study the bonding characters of some selected structures. The Gibbs free energies were calculated in the gas phase using the Gaussian09 package with the formulas  $H = E + RT$ ,  $G = H - TS$ , where  $H$  is the enthalpy and  $S$  is the entropy.

Double- $\square$  plus polarization (DZP) basis sets were used for the DFT optimizations in this research. For carbon one set of pure spherical harmonic d functions with orbital exponent  $\square_d(C) = 0.75$  is added to the standard

Huzinaga-Dunning contracted DZ sets. This basis set is designated (9s5p1d/4s2p1d).<sup>26,27</sup> For hydrogen, a set of p polarization functions  $\square_p(\text{H}) = 0.75$  is added to the Huzinaga-Dunning DZ sets. For the transition metals, in our loosely contracted DZP basis sets, the Wachters' primitive sets are used, but augmented by two sets of p functions and one set of d functions, contracted following Hood *et al.*, and designated (14s11p6d/10s8p3d).<sup>28,29</sup>

The geometries of all structures were fully optimized by using the above two DFT methods with the (120, 974) integration grid. Small imaginary frequencies were assumed to arise for the optimized structures because of numerical integration errors. For benchmarking the results with DFT methods and DZP basis sets, the single point energies for some selected structures were also computed by the much higher level DLPNO-CCSD(T)/def2-TZVP method<sup>30,31</sup> implemented in the ORCA program<sup>32</sup> and the B3PW91-D3/def2-TZVP method in Gaussian 09 program based on the geometries obtained by the  $\square$ B97xD /DZP method.

### 3. Results and Discussion

#### 3.1 Dissociation of $\text{R}_4\text{Fe}$ (R = cx and nor)

The present computations predict that the lowest energy (cx)<sub>4</sub>Fe structure has  $S_4$  symmetry corresponding to a highly symmetrical tetrahedral coordination environment. However, the more reliable DLPNO-CCSD(T)/def2-TZVP method predicts a triplet (cx)<sub>4</sub>Fe structure with  $D_2$  symmetry to lie only 1.2 kcal/mol lower than its highly symmetric singlet structure. A quintet energy (cx)<sub>4</sub>Fe structure is found to lie only 3.1 kcal/mol in energy above its singlet isomer (Table 1). These calculations suggest a close separation between potential energy surfaces of different spins.

In the corresponding predicted singlet (nor)<sub>4</sub>Fe structure, the tetrahedral coordination of the 1-norbornyl groups to the central iron atom is slightly distorted. Both DFT methods and the more accurate DLPNO-CCSD(T)/def2-TZVP method predict this singlet (nor)<sub>4</sub>Fe structure to be the lowest energy structure consistent with the experimental observation of its diamagnetism. The  $\square$ B97XD/DZP method predicts the triplet and quintet spin states of (nor)<sub>4</sub>Fe to lie 6.9 and 12.0 kcal/mol, respectively, above the singlet isomer (Table 2). The DLPNO-CCSD(T)/def2-TZVP method predicts only slightly higher energies for the higher spin states of (nor)<sub>4</sub>Fe, namely, 2.4 and 3.9 kcal/mol for the triplet and quintet states, respectively (Table 1).

Two possible dissociation schemes for these  $\text{R}_4\text{Fe}$  derivatives have been suggested (Figure 2). These relate to understanding the widely different thermal stabilities of (cx)<sub>4</sub>Fe and (nor)<sub>4</sub>Fe. In order to evaluate these dissociation schemes, optimization of the dissociation products  $\text{R}_3\text{Fe}$  and  $\text{R}_2\text{Fe}$  (R = cx and nor) is required.

For  $(cx)_3Fe$ , all methods used in the present study predict the quartet state to be lower in energy than the doublet state. For the  $(cx)_2Fe$  structure, the quintet state is predicted to be the ground state by both DFT methods and the DLPNO-CCSD(T)/def2-TZVP method (Table 2). The dissociation fragments for the two proposed dissociation schemes are neutral, and the reactants and products have different spin states. Dissociation from the experimentally known singlet tetraalkyl  $(cx)_4Fe$  or  $(nor)_4Fe$  structures to the neutral dialkyl fragments  $(cx)_2Fe$  or  $(nor)_2Fe$  in the energetically preferred quintet spin state or the trialkyl fragments  $(cx)_3Fe$  or  $(nor)_3Fe$  in the energetically preferred quartet state requires spin flipping. Such reactions will occur through a conical-intersection with a crossing region between the different spin states of the tetraalkyls  $(cx)_4Fe$  or  $(nor)_4Fe$ .

**Table 1.** Relative energies (in kcal/mol) for different spin states of the  $(cx)_nFe$  ( $n = 4, 3, 2$ ) structures with the lowest energy structures indicated in **bold**.

		$\Delta E$ (kcal/mol)	
		$\square$ B97XD/DZP	DLPNO-CCSD(T)/ def2-TZVP*
$(cx)_4Fe$	<b>Singlet</b>	<b>0.0</b>	0.0
	<b>Triplet</b>	3.7	<b>-1.2</b>
	Quintet	12.2	3.1
$(cx)_3Fe$	Doublet	6.3	10.4
	<b>Quartet</b>	<b>0.0</b>	<b>0.0</b>
$(cx)_2Fe$	Singlet	57.3	66.9
	Triplet	15.3	31.2
	<b>Quintet</b>	<b>0.0</b>	<b>0.0</b>

\*The energies are computed as the single point energies from the geometries of  $\square$ B97XD/DZP method.

**Table 2.** Relative energy differences (in kcal/mol) for different spin states of  $(cx)_4Fe$  and  $(nor)_4Fe$ .

	$(cx)_4Fe$		$(nor)_4Fe$	
	$\square$ B97XD/ DZP	DLPNO-CCSD(T)/ def2-TZVP*	$\square$ B97XD/ DZP	DLPNO-CCSD(T)/ def2-TZVP*
<b>Singlet (Exp.)</b>	<b>0.0</b>	<b>0.0</b>	<b>0.0</b>	<b>0.0</b>
Triplet	3.7	-1.2	6.9	2.4
Quintet	12.2	3.1	12.0	3.9

\*The energies are computed as the single point energies from the geometries of  $\square$ B97XD/DZP method.

Removal of one cyclohexyl ligand from  $(cx)_4Fe$  by the reaction  $(cx)_4Fe \square (cx)_3Fe + cx\bullet$  is an endothermic process requiring 38.8 kcal/mol

(DLPNO-CCSD(T)/def2-TZVP). However, dissociation of cyclohexyl dimer cx-cx from  $(cx)_4Fe$  by the reaction  $(cx)_4Fe \rightarrow (cx)_2Fe + cx-cx$  is an exothermic process, releasing 22.9 kcal/mol (DLPNOCCSD(T)/def2-TZVP). These thermochemical results for the above two reactions suggest that dissociation of  $(cx)_4Fe$  through the second scheme by elimination of cx-cx is more probable than that through the first scheme by elimination of  $cx\cdot$  (Table 3).

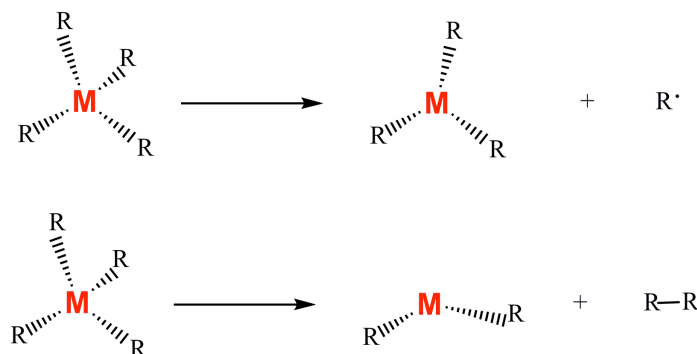


**Figure 2.** Two proposed dissociation schemes for the  $R_4M$  structures, where **M** = transition metal and R = 1-norbornyl (nor) or cyclohexyl (cx).

**Table 3.** Dissociation energies (in kcal/mol) for the reactions  $(cx)_4Fe \rightarrow (cx)_3Fe + cx\cdot$  and  $(cx)_4Fe \rightarrow (cx)_2Fe + cx-cx$  predicted at different theoretical levels.

$(cx)_4Fe \rightarrow (cx)_3Fe + cx\cdot$							
DLPNO-CCSD(T) <sup>a</sup>	$\square$ B97XD	B3PW91-D3 <sup>b</sup>		B3PW91		$\Delta E(-D3)$	
def2-TZVP	DZP	DZP	def2-TZVP	DZP	Def2-TZVP <sup>b</sup>	DZP	def2-TZVP
<b>38.8</b>	43.3	53.5	46.3	34.8	29.3	18.7	<b>17.0</b>
$(cx)_4Fe \rightarrow (cx)_2Fe + cx-cx$							
DLPNO-CCSD(T) <sup>a</sup>	$\square$ B97XD	B3PW91-D3 <sup>b</sup>		B3PW91		$\Delta E(-D3)$	
def2-TZVP	DZP	DZP	def2-TZVP	DZP	Def2-TZVP <sup>b</sup>	DZP	def2-TZVP
<b>-22.9</b>	-12.0	5.1	1.2	-15.7	-19.6	20.8	<b>20.8</b>

<sup>a</sup> The energies are computed as the single point energies from the geometries of the  $\square$ B97XD/DZP method.

<sup>b</sup> The energies are computed as the single point energies from the geometries of the B3PW91/DZP method.

Similar dissociation energies are predicted for  $(nor)_4Fe$  (Table 4). Thus dissociation of  $(nor)_4Fe$  by eliminating  $nor\cdot$  is endothermic by 41.5 kcal/mol (DLPNO-CCSD(T)/def2-TZVP). However, dissociation of 1-norbornyl dimer nor-nor from  $(nor)_4Fe$  by the reaction  $(nor)_4Fe \rightarrow (nor)_2Fe + nor-nor$  is exothermic, releasing 27.4 kcal/mol (DLPNOCCSD(T)/def2-TZVP. The  $\square$ B97XD/DZP method predicts more consistent dissociation energies with the more reliable DLPNO-CCSD(T)/def2-TZVP method. However, the B3PW91/def2-TZVP method predicts better energy differences for dissociation of  $R_4Fe$  to  $R_2Fe + R_2$  and bad dissociation energies for dissociation of  $R_4$  to  $R_3Fe + R\cdot$ . These benchmarking studies indicate the suitability of DFT methods with DZP basis sets for investigating dispersion effects in  $R_4Fe$  dissociation reactions.

The cyclohexyl derivative (cx)<sub>4</sub>Fe was observed to be unstable at temperatures above -20 °C. However, the norbornyl derivative (nor)<sub>4</sub>Fe was observed by Bower and Tennent<sup>5</sup> to be stable up to 23 °C.<sup>5</sup> The thermodynamics of the exothermic reactions R<sub>4</sub>Fe → R<sub>2</sub>Fe + R-R are related to the stabilities of the two different Fe(IV) compounds (cx)<sub>4</sub>Fe and (nor)<sub>4</sub>Fe. The potential energy surfaces of different spin states of the (cx)<sub>4</sub>Fe structure containing the key structures were calculated by the  $\square$ B97XD/DZP and DLPNO-CCSD(T)/def2-TZVP methods. For the singlet potential energy surface, a very high barrier of 82.7 kcal/mol (Figure 3a) was predicted for the (cx)<sub>4</sub>Fe → (cx)<sub>2</sub>Fe + cx-cx reaction by the more accurate DLPNO-CCSD(T)/def2-TZVP method (Figure 3a). A lower reaction barrier of 42.6 kcal/mol is calculated for the triplet spin states of (cx)<sub>4</sub>Fe at the same theoretical level. An even lower reaction barrier of 18.1 kcal/mol was predicted by the DLPNO-CCSD(T)/def2-TZVP method for the quintet potential energy surface of (cx)<sub>4</sub>Fe.

**Table 4.** Dissociation energies (in kcal/mol) for the reactions (nor)<sub>4</sub>Fe → (nor)<sub>3</sub>Fe + nor• and (nor)<sub>4</sub>Fe → (nor)<sub>2</sub>Fe + nor-nor predicted by at different theoretical levels.

(nor) <sub>4</sub> Fe → (nor) <sub>3</sub> Fe + nor•							
DLPNO-CCSD(T)*	B3PW91-D3 <sup>b</sup>			B3PW91		ΔE(-D3)	
def2-TZVP	DZP	DZP	def2-TZVP	DZP	Def2-TZVP <sup>b</sup>	DZP	def2-TZVP
<b>41.5</b>	47.7	56.5	53.1	31.3	27.6	25.4	<b>25.5</b>
(nor) <sub>4</sub> Fe → (nor) <sub>2</sub> Fe + nor-nor							
DLPNO-CCSD(T)	B3PW91-D3 <sup>b</sup>			B3PW91		ΔE(-D3)	
def2-TZVP	DZP	DZP	def2-TZVP	DZP	Def2-TZVP <sup>b</sup>	DZP	def2-TZVP
<b>-27.4</b>	-5.6	2.2	-1.8	-29.3	-33.3	31.5	<b>31.5</b>

<sup>a</sup> The energies are computed as the single point energies from the geometries of the  $\square$ B97XD/DZP method.

<sup>b</sup> The energies are computed as the single point energies from the geometries of the B3PW91/DZP method.

Similar barriers for the (nor)<sub>4</sub>Fe → (nor)<sub>2</sub>Fe + nor-nor dissociation process decreasing with increasing spin states are predicted for the (nor)<sub>4</sub>Fe compounds (Figure 3b). Thus the barrier for decomposition of quintet (nor)<sub>4</sub>Fe is even lower, namely 14.2 kcal/mol at the DLPNO-CCSD(T)/def2-TZVP level, than that of quintet (cx)<sub>4</sub>Fe. This would seem to suggest that (nor)<sub>4</sub>Fe should be less stable than (cx)<sub>4</sub>Fe because of the lower reaction barrier in the quintet state. However, the geometry of quintet (cx)<sub>4</sub>Fe with D<sub>2</sub> symmetry is distorted significantly from that of singlet (cx)<sub>4</sub>Fe with S<sub>4</sub> symmetry and an almost ideal tetrahedral coordination of the central iron atom as determined by X-ray crystallography. In contrast, the high spin (nor)<sub>4</sub>Fe geometry is not as significantly distorted from that in the singlet (nor)<sub>4</sub>Fe structure than that for quintet (cx)<sub>4</sub>Fe. This suggests that constraints resulting from the steric repulsions and

the dispersion attractions among different ligands in the tetraalkyliron compounds  $(\text{nor})_4\text{Fe}$  and  $(\text{cx})_4\text{Fe}$  determine their relative stabilities. If the  $\text{R}_4\text{Fe} \rightarrow \text{R}_2\text{Fe} + \text{R-R}$  dissociation scheme is possible, a spin-flip is needed at the conical intersection in the crossing region. For  $(\text{cx})_4\text{Fe}$ , the slightly higher energy quintet state structure may force the experimentally determined singlet structure to relax and cross with the quintet potential surface having a lower reaction barrier than the value of 18.1 kcal/mol predicted by the DLPNO-CCSD(T)/def2-TZVP method. For  $(\text{nor})_4\text{Fe}$ , the more sterically demanding norbornyl ligand and the stronger dispersion attraction among the norbornyl ligands leads to little distortion of the structure in going from the singlet to the quintet spin state. Therefore, the conical intersection between the singlet potential surface and the high spin potential surface may not be relevant. As a result, the much higher barrier for the  $(\text{nor})_4\text{Fe} \rightarrow (\text{nor})_2\text{Fe} + \text{nor-nor}$  dissociation makes the experimentally known  $(\text{nor})_4\text{Fe}$  more resistant towards such dissociation.

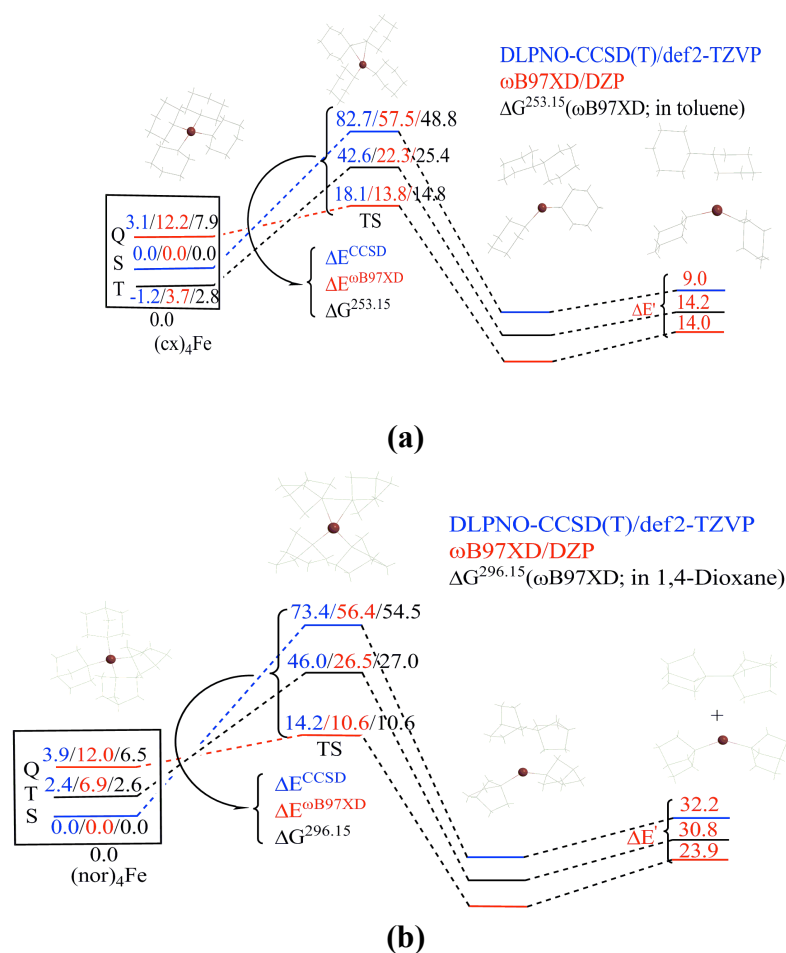


**Figure 3.** The reaction paths of the  $\text{R}_4\text{M} \rightarrow \text{R}_2\text{M} + \text{R-R}$  dissociation scheme for (a) the  $(\text{cx})_4\text{Fe}$  structure, and (b) the  $(\text{nor})_4\text{Fe}$  structure. ( $\Delta\text{E}$  and  $\Delta\text{G}$  are the reaction energy and Gibbs free energy barriers and  $\Delta\text{E}'$  is the energy difference between the exit complex and the free products).

The dispersion effect in stabilizing the  $R_4M$  derivatives ( $R = \text{cx}$  or  $\text{nor}$ ;  $M = \text{Ti}$  to  $\text{Ni}$ ) compounds was studied by the B3PW91-D3/DZP method (Tables 5 to 8 and Figure 4). The results show that the energy lowering from the dispersion attraction is more significant in the  $(\text{nor})_4M$  compounds than in the  $(\text{cx})_4M$  compounds. This may be caused by the larger size and steric effect of the norbornyl ligand relative to the cyclohexyl ligand. For the dissociation scheme  $(\text{cx})_4M \rightarrow (\text{cx})_3M + \text{cx}\cdot$ , the dispersion stabilization energy ranges from 12.5 kcal/mol for  $(\text{cx})_4\text{Ni}$  to 24 kcal/mol for  $(\text{cx})_4\text{Fe}$ . For the dissociation scheme  $(\text{nor})_4M \rightarrow (\text{nor})_3M + \text{nor}\cdot$  the dispersion energies range from 18.2 kcal/mol for  $(\text{nor})_4\text{Cr}$  to 25.4 kcal/mol for  $(\text{nor})_4\text{Fe}$ . For the  $R_4M \rightarrow R_2M + R-R$  dissociation scheme, the stabilizing energies in the  $(\text{cx})_4M$  compounds range from 13.4 kcal/mol for  $(\text{cx})_4\text{Cr}$  to 20.8 kcal/mol for  $(\text{cx})_4\text{Fe}$ . However, for the  $(\text{nor})_4M$  derivatives such stabilizing energy ranges from 19.0 kcal/mol for  $(\text{nor})_4\text{Ti}$  to 31.5 kcal/mol for  $(\text{nor})_4\text{Fe}$ . The stabilizing energy from the dispersion effect in the experimentally known  $(\text{nor})_4\text{Fe}$  is 10.7 kcal/mol larger than that in  $(\text{cx})_4\text{Fe}$  in terms of the  $R_4M \rightarrow R_2M + R-R$  dissociation process. This indicates a particularly strong dispersion effect among the norbornyl ligands.

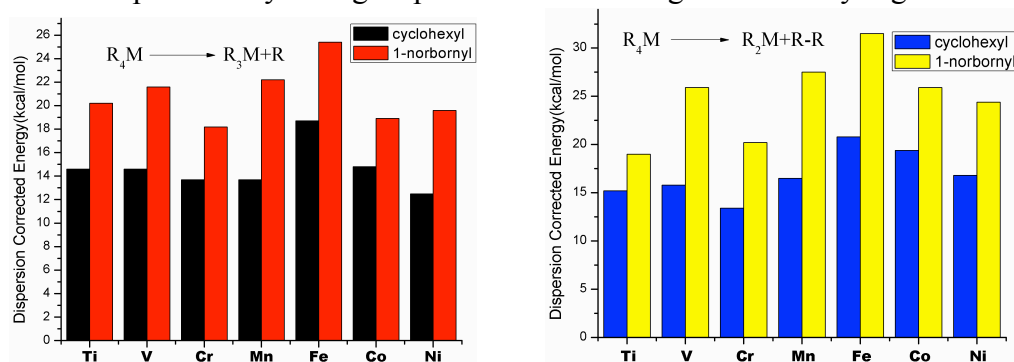


**Figure 4.** Dispersion corrected energies for the dissociation schemes  $R_4M \rightarrow R_3M + R\cdot$  and  $R_4M \rightarrow R_2M + R-R$  ( $M = \text{Ti}$  to  $\text{Ni}$ ) predicted at the B3PW91/DZP level.

**Table 5.** Dissociation energies for the reactions  $(\text{cx})_4M \rightarrow (\text{cx})_3M + \text{cx}\cdot$  (kcal/mol).

	$(\text{cx})_4M \rightarrow (\text{cx})_3M + \text{cx}\cdot$			
	B3PW91-D3	B3PW91 <sup>a</sup>	$\Delta E(-D3)$ <sup>b</sup>	$\square$ B97XD
Ti	66.9	52.3	14.6	67.3
V	58.0	43.4	14.6	56.5
Cr	48.3	34.6	13.7	50.0
Mn	33.8	20.1	13.7	34.3
<b>Fe</b>	<b>53.5</b>	<b>34.9</b>	<b>18.7</b>	<b>43.3</b>
Co	41.1	26.3	14.8	38.3
Ni	29.5	17.0	12.5	29.5
<b>Ru</b>	<b>69.3</b>	<b>55.8</b>	<b>14.5</b>	<b>69.7</b>
<b>Os</b>	<b>79.6</b>	<b>63.6</b>	<b>16.0</b>	<b>78.7</b>

**Table 6.** Dissociation energies (in kcal/mol) for the reactions  $(cx)_4M \rightarrow (cx)_2M + cx-cx$ .

	$(cx)_4M \rightarrow (cx)_2M + cx-cx$			
	B3PW91-D3	B3PW91 <sup>a</sup>	$\Delta E(-D3)$ <sup>b</sup>	$\square$ B97XD
Ti	52.3	37.1	15.2	38.5
V	25.8	10.0	15.8	21.3
Cr	4.0	-9.4	13.4	6.0
Mn	-15.9	-32.4	16.5	-20.5
<b>Fe</b>	<b>5.1</b>	<b>-15.7</b>	<b>20.8</b>	<b>-12.0</b>
Co	-3.7	-23.1	19.4	-6.0
Ni	-20.8	-37.6	16.8	-27.5
<b>Ru</b>	<b>44.7</b>	<b>29.3</b>	<b>15.4</b>	<b>42.5</b>
<b>Os</b>	<b>63.6</b>	<b>43.2</b>	<b>20.4</b>	<b>55.1</b>

**Table 7.** Dissociation energies for the reactions  $(nor)_4M \rightarrow (nor)_3M + nor\bullet$  (kcal/mol).

	$(nor)_4M \rightarrow (nor)_3M + nor\bullet$			
	B3PW91-D3	B3PW91	$\Delta E(-D3)$	$\square$ B97XD
Ti	77.1	56.9	20.2	77.7
V	66.0	44.4	21.6	64.8
Cr	56.5	38.3	18.2	58.7
Mn	46.8	24.6	22.2	45.1
<b>Fe</b>	<b>56.5</b>	<b>31.1</b>	<b>25.4</b>	<b>47.7</b>
Co	43.5	24.6	18.9	41.5
Ni	37.2	17.6	19.6	35.7

**Table 8.** Dissociation energies for the reactions  $(nor)_4M \rightarrow (nor)_2M + nor-nor$  (kcal/mol).

	$(nor)_4M \rightarrow (nor)_2M + nor-nor$			
	B3PW91-D3	B3PW91	$\Delta E(-D3)$	$\square$ B97XD
Ti	41.3	22.3	19.0	40.2
V	23.4	-2.5	25.9	21.6
Cr	3.3	-16.9	20.2	5.8
Mn	-13.6	-41.1	27.5	-20.3
<b>Fe</b>	<b>2.2</b>	<b>-29.3</b>	<b>31.5</b>	<b>-5.6</b>
Co	-10.9	-36.8	25.9	9.2
Ni	-25.2	-49.6	24.4	-31.3

In these high-valent compounds, there are strong Coulombic interactions owing to the high charge density located on the metal atoms. This kind of interaction

may also affect the stabilities of the present tetraalkylmetal compounds. In this connection, energy decomposition analysis (EDA) was performed using Shubin Liu's scheme<sup>33</sup> implemented in Multiwfn,  $E = E_{steric} + E_{electrostatic} + E_{quantum}$ , at the B3PW91/DZP level. The electrostatic term is the sum of all classical Coulomb interactions of the particles in the system:

$$E_{electrostatic} = E_J + E_{N-E} + E_{E-E}$$

$$= \iint \frac{\rho(r_1^V)\rho(r_2^V)}{r_{12}} dr_1^V dr_2^V - \int \rho(r^V) \sum_A \frac{Z_A}{r - R_A} dr^V + \sum_{A>B} \frac{Z_A Z_B}{R_{AB}}$$

This calculation indicates (Figure 5) that for the early transition metals the Coulombic interactions contribute much more to stabilize the tetraalkylmetal derivatives than the dispersion effect with respect to the dissociation schemes  $R_4M \rightarrow R_3M + R\bullet$  and  $R_4M \rightarrow R_2M + R-R$ . The contribution from the Coulombic interactions almost monotonically decreases with increasing atomic number of the transition metal atom. For the cobalt and nickel compounds, the contributions from both effects are comparable so that even the electrostatic effect destabilizes the  $(cx)_4Ni \rightarrow (cx)_2Ni + cx-cx$  reaction. This may relate to the emptier *d* orbitals of the early transition metals to attract more electrons from the surrounding ligands thereby increasing the electrostatic interaction between the central metal and the alkyl groups. The results also suggest that the energy lowering from the Coulombic interactions is much more significant in the  $(nor)_4M$  compounds than in the  $(cx)_4M$  compounds. The Coulombic interactions may play a more important role in stabilizing the tetraalkylmetal compounds than that for the dispersion effect.

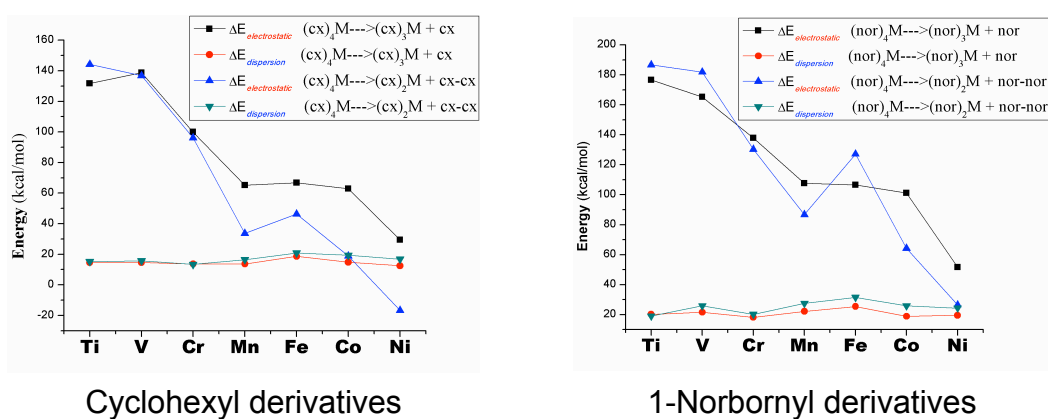


**Figure 5.** Contributions from the electrostatic effect and the dispersion effect to the dissociation energies of  $R_4M \rightarrow R_3M + R\bullet$  and  $R_4M \rightarrow R_2M + R-R$  ( $M=Ti$  to  $Ni$ ;  $R=cx$  or  $nor$ ) predicted at the B3PW91/DZP level.

### 3.2 Comparison of (cx)<sub>4</sub>Fe with its ruthenium and osmium analogues (cx)<sub>4</sub>M (M = Ru, Os)

The metal-carbon distances are almost equal for the experimentally known (cx)<sub>4</sub>M (M = Fe,<sup>7</sup> Ru<sup>16</sup>, or Os<sup>16</sup>) structures of the group 8 metals. This suggests that the dispersion energies should change very little in going from iron to ruthenium and then osmium. Therefore the exceptionally high stability of the experimentally known isostructural (cx)<sub>4</sub>M (M = Ru, Os)<sup>16</sup> must result mainly from the larger ligand field splittings for the 4d transition metal ruthenium and the 5d transition metal osmium relative to their 3d congener iron. As a result the singlet-triplet splittings for the ruthenium and osmium derivatives (cx)<sub>4</sub>M (M = Ru, Os) are much larger than those for (cx)<sub>4</sub>Fe (Table 9). Thus the isostructural derivative (cx)<sub>4</sub>Os of the 5d transition metal osmium is thermally stable up to 200 °C without any C-C or C-H hydride elimination.<sup>16</sup> The energies for the dissociation schemes (cx)<sub>4</sub>M → (cx)<sub>3</sub>M + cx• and (cx)<sub>4</sub>M → (cx)<sub>2</sub>M + cx-cx (M = Ru, Os) are all significantly endothermic (Tables 5 to 8). However, for the analogous 3d transition metal derivative (cx)<sub>4</sub>Fe, the energy for the corresponding (cx)<sub>4</sub>Fe → (cx)<sub>2</sub>Fe + cx-cx dissociation process is predicted to be greatly exothermic at 22.9 kcal/mol by DLPNO-CCSD(T)/def2-TZVP. The seriously distorted D<sub>2</sub> triplet (cx)<sub>4</sub>Ru and (cx)<sub>4</sub>Os structures are much higher in energies than their highly symmetric S<sub>4</sub> singlet isomers (Table 9). In contrast, the distorted high spin triplet or quintet (cx)<sub>4</sub>Fe structures are almost energetically degenerate with its high symmetric S<sub>4</sub> singlet isomer. The significantly higher relative energies of the high spin potential energy surfaces of (cx)<sub>4</sub>M (M = Ru, Os) preclude the conical intersection between the singlet potential surface and the high spin potential surfaces. This keeps the (cx)<sub>4</sub>Ru and (cx)<sub>4</sub>Os species on their lowest energy singlet potential surfaces, thereby hindering dissociation to cx-cx because of the very high reaction barrier. The predicted dissociation energies for the scheme (cx)<sub>4</sub>M → (cx)<sub>3</sub>M + cx• for ruthenium and osmium are also significantly larger than those for the corresponding iron species, (cx)<sub>4</sub>Fe. This suggests the remarkable stability of the (cyl)<sub>4</sub>Ru and (cyl)<sub>4</sub>Os compounds in terms of single ligand dissociation.

**Table 9.** Energy differences between the triplet (D<sub>2</sub>) and singlet (S<sub>4</sub>) (cx)<sub>4</sub>M (M = Fe, Ru, Os) structures.

	ΔE [Triplet–Singlet] (kcal/mol)	
	B3PW91-D3/DZP	□B97XD/DZP
(cx) <sub>4</sub> Fe	2.0	3.7
(cx) <sub>4</sub> Ru	33.9	33.6
(cx) <sub>4</sub> Os	42.9	36.2

### 3.3 Analysis of the frontier molecular orbitals of $R_4Fe$ ( $R = cx$ and $nor$ ).

The singlet  $(nor)_4Fe$  and  $(cx)_4Fe$  structures have similar frontier orbitals displaying the interactions between the alkyl group ( $nor$  or  $cx$ ) and the central iron atom (Figures 6 and 7). The central iron atom forms tetrahedrally disposed Fe–C bonds to the four surrounding alkyl groups through its  $d_{xy}$ ,  $d_{yz}$ , and  $d_{zx}$ , orbitals. Orbital decomposition analysis indicates that the main contribution to the four Fe–C bonds arise from the  $p$  orbitals of the carbon atoms directly bonded to the iron atom (Figure 8). The predicted iron-carbon distances are close to the experimentally measured values, and their Wiberg bond Indices (WBIs) are all 0.89, suggesting strong covalent interactions between the central iron atom and the four adjacent carbon atoms (Table 10). The iron  $d_z^2$  and  $d_{x^2-y^2}$  orbitals contribute more than 50% of the non-bonding HOMO and HOMO-1 orbitals within the singlet structure  $(cx)_4Fe$  (Figure 8). Similar results were predicted for the singlet structure  $(nor)_4Fe$ .

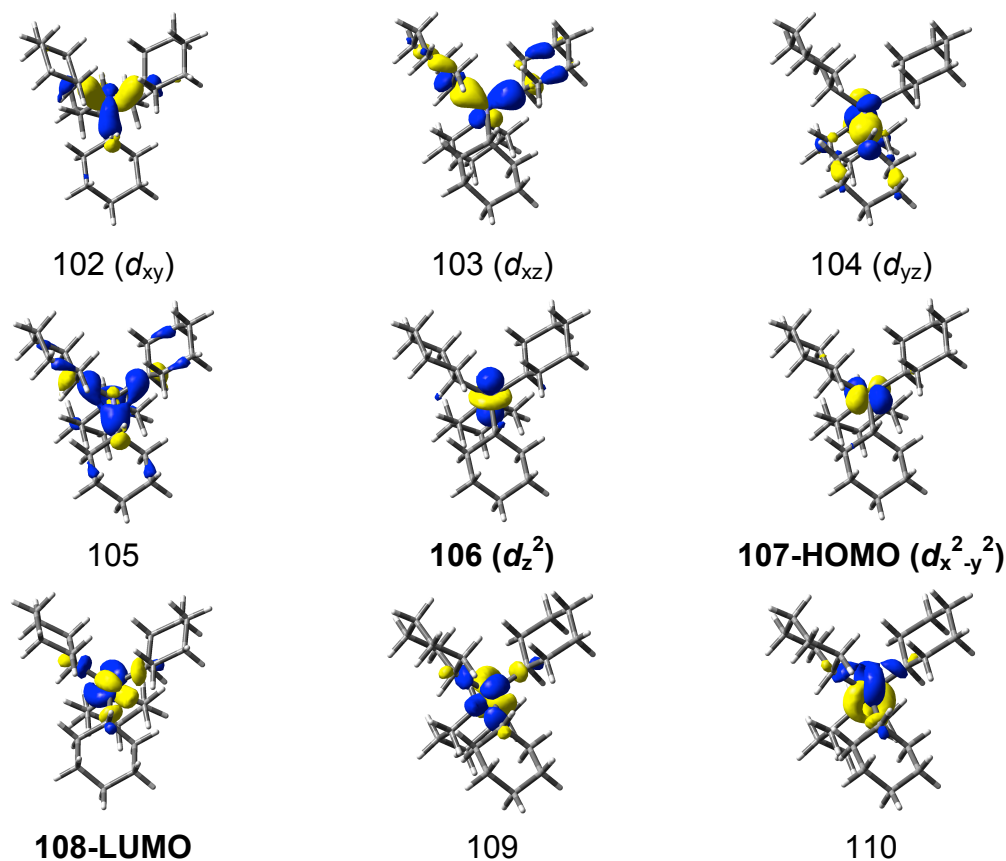


**Figure 6.** Frontier molecular orbitals of the singlet  $(cx)_4Fe$  structure with  $S_4$  symmetry obtained at the  $\square B97XD/DZP$  level. (The isovalue is 0.06)

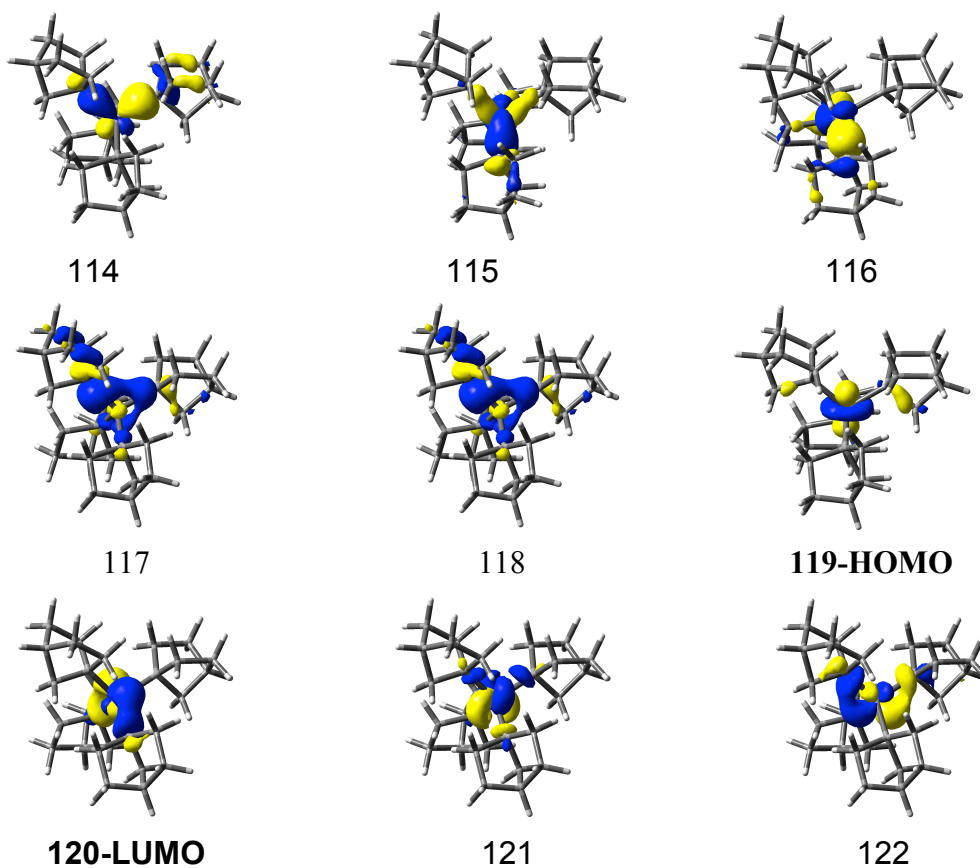


**Figure 7.** Frontier molecular orbitals of the singlet  $(\text{nor})_4\text{Fe}$  structure with the experimentally obtained  $C_s$  symmetry obtained at the  $\square\text{B97XD/DZP}$  level. (The isovalue is 0.06).

The  $(\text{cx})_4\text{M}$  complexes of the metals adjacent to iron in the Periodic Table deviate from ideal symmetry owing to the Jahn-Teller effect. Thus in the lowest energy quartet spin state structure of the manganese derivative  $(\text{cx})_4\text{Mn}$  one electron is excited into an antibonding orbital containing a  $d_{xy}$ ,  $d_{yz}$ , or  $d_{zx}$  component. Similarly one antibonding orbital containing the  $d_{xy}$ ,  $d_{yz}$ , or  $d_{zx}$  component is occupied in the doublet  $(\text{cx})_4\text{Co}$  structure and the singlet  $(\text{cx})_4\text{Ni}$  structure. These partially filled orbitals lead to the Jahn-Teller effect splitting the triply degenerate  $\{d_{xy}, d_{yz}, d_{zx}\}$  set of an ideal tetrahedral structure so that the lowest energy  $(\text{cx})_4\text{M}$  ( $\text{M} = \text{Mn}, \text{Co},$  and  $\text{Ni}$ ) structures deviate significantly from such ideal tetrahedral symmetry. Similar coordination environments as in the cyclohexyl derivatives  $(\text{cx})_4\text{M}$  ( $\text{M} = \text{Ti}$  to  $\text{Ni}$ ) are also predicted for the gas phase  $(\text{nor})_4\text{M}$  ( $\text{M} = \text{Ti}$  to  $\text{Ni}$ ) structures.

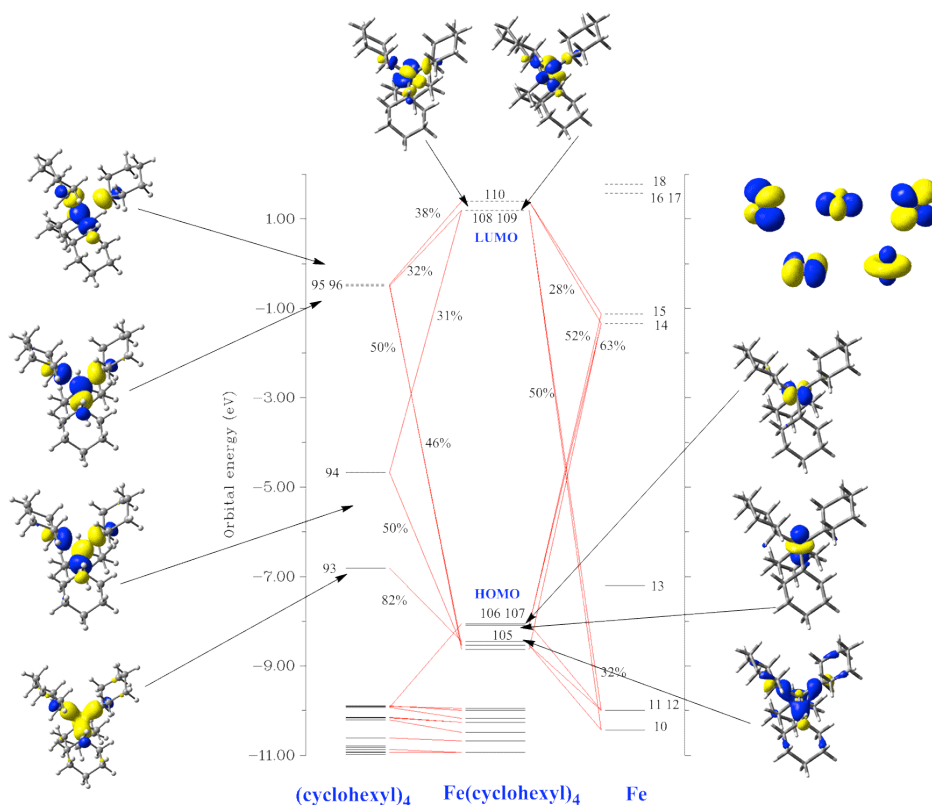


**Figure 8.** Orbital decomposition analysis for the singlet  $(cx)_4Fe$  structure with  $S_4$  symmetry obtained at the  $\square B97XD/DZP$  level.

**Table 10.** Comparisons of the Fe-C bond lengths (in Å) between the experimental<sup>7</sup> and theoretical singlet  $(cx)_4Fe$  structures and their Wiberg Bond Indexs (WBIs).

	Exp. (in Å)	Theo. (in Å)	WBIs
Fe-C1	1.931	1.908	0.89
Fe-C2	1.928	1.908	0.89
Fe-C3	1.931	1.908	0.89
Fe-C4	1.928	1.908	0.89

**NBO charge on Fe: 0.279**

### 3.4 Comparison of the reactivities of $(cx)_4Fe$ and $(nor)_4Fe$ towards carbon monoxide.

The dispersion effect in stabilizing the experimentally synthesized structures  $(nor)_4Fe$  and  $(cx)_4Fe$  can also relate to reactivity with small molecules. Little indication is given in earlier work<sup>2,3</sup> that the  $(cx)_4Fe$  structure is observed to be much less stable than the  $(nor)_4Fe$  structure, owing to the reduced dispersion effect resulting from smaller cyclohexyl groups relative to 1-norbornyl groups. However, a detailed study on the mechanism has been performed. The more exposed Fe(IV) center of the  $(cx)_4Fe$  structure is much more accessible to bind suitable small molecules. As an example the absorption of carbon monoxide on the substrate  $(cx)_4Fe$  and  $(nor)_4Fe$  was investigated. The results suggest that CO can be weakly bound to the Fe(IV) center

in the  $(\text{cx})_4\text{Fe}$  structure as a terminal ligand followed by migratory insertion into an Fe–C bond with only a small energy barrier of 7.4 kcal/mol ( $\square\text{B97XD/DZP}$ ). This leads to a structure with a carbonyl group bridging the central iron atom to a cyclohexyl group (**Figure 9**). Similar reactions have been observed for alkylimide migratory insertions in the Fe(IV) complex  $(\text{Me}_2\text{IPr})\text{Fe}(=\text{NAd})\text{R}_2$  (Ad = adamantyl; R = neopentyl, 1-nor)<sup>34,35</sup> and CO insertion in oxorhenium hydrides.<sup>36</sup> Reaction of the singlet CO insertion product  $(\text{cx})_3\text{Fe}(\text{COcx})$  with a second CO molecule is also predicted to be possible (**Figure 10**). Such a reaction results in migration into the Fe–C(CO) bond when climbing over the relatively higher energy barrier of 26.3 kcal/mol ( $\square\text{B97XD/DZP}$ ) analogous to the coupling of two carbonyl groups observed in the Re(III) complex<sup>37</sup>. The second terminally bound CO group could also migrate to insert into another Fe–C(cx) bond. A similar migratory insertion reaction is also possible for the third CO group, which has a comparable energy barrier to the second CO group (**Figure 11**). If  $\text{O}_2$  and  $\text{N}_2$  could overcome the repulsion force from the ligands and reach the central iron atom, the possible structures may be as shown in **Figure 12**, in which the two molecules both function as the bridging groups between the central iron atom and one cyclohexyl group. If those things happened, the double bond in the  $\text{O}_2$  molecule could be reduced to a single bond of length 1.435 Å. However, the N–N bond length in  $\text{N}_2$  could only be reduced slightly with a nitrogen-nitrogen distance of 1.206 Å. In contrast to the  $(\text{cx})_4\text{Fe}$  system, the present study shows that carbon monoxide cannot penetrate the tightly bound sphere of the  $(\text{nor})_4\text{Fe}$  structure owing to the strong dispersion forces. This shows that even small molecules cannot easily penetrate the outer hydrocarbon protective layer in  $(\text{nor})_4\text{Fe}$  to reach the central high-valent iron atom. This accounts for the lower chemical reactivity of  $(\text{nor})_4\text{Fe}$  relative to  $(\text{cx})_4\text{Fe}$ .

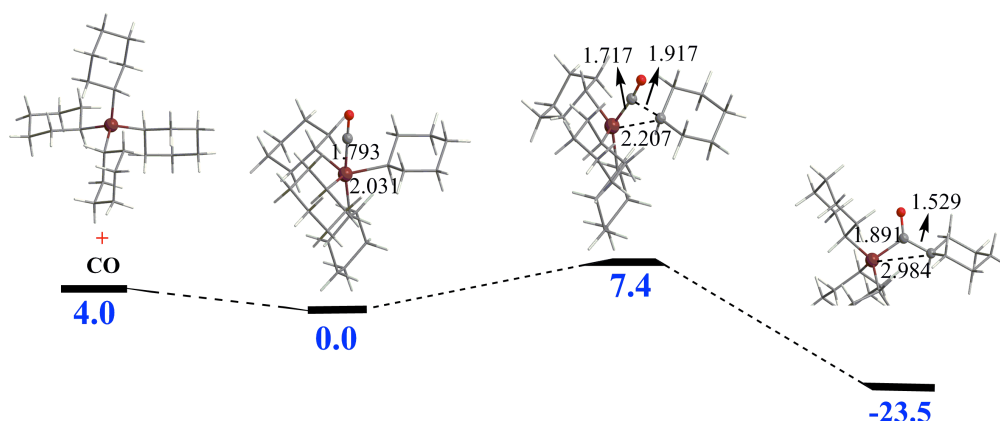


**Figure 9.** The CO absorption reaction paths for the singlet  $(\text{cx})_4\text{Fe}$  structure calculated at the  $\square\text{B97XD/DZP}$  level.

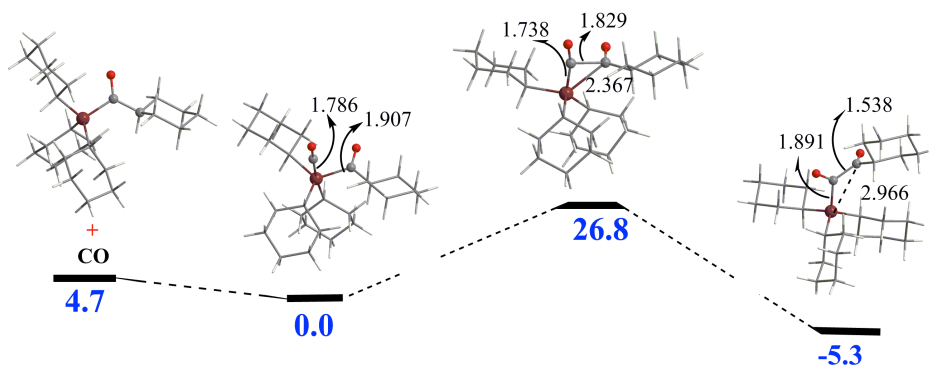


**Figure 10.** Reaction of the singlet  $(cx)_3Fe(COcx)$  structure with a second CO ligand from the  $\square B97XD/DZP$  method.

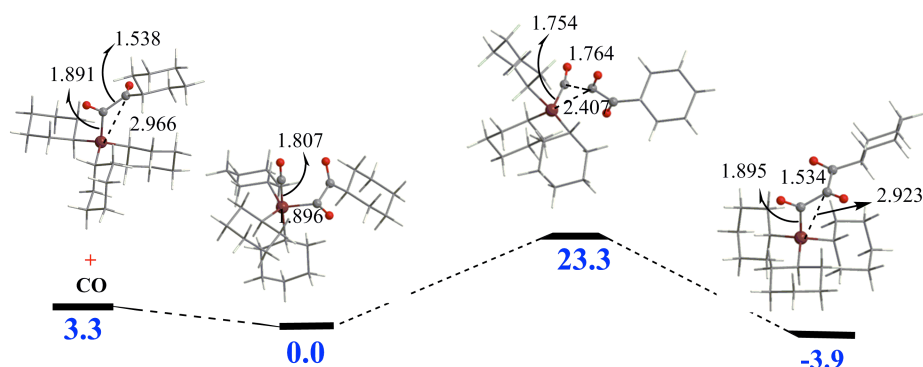


**Figure 11** Reaction of the singlet  $(cx)_3Fe(C_2O_2cx)$  structure with a third CO ligand evaluated at the  $\square B97XD/DZP$  level.

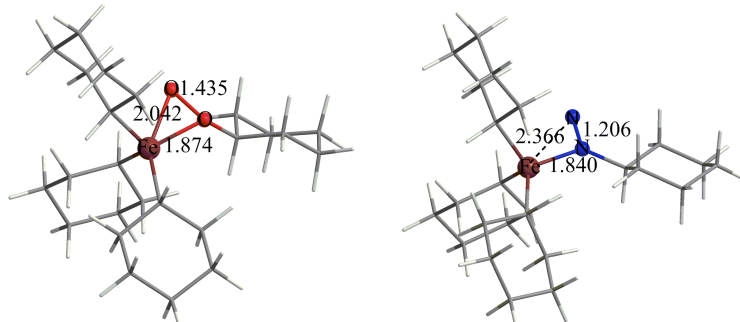


**Figure 12** Possible absorption mode of the  $O_2$  and  $N_2$  molecules on the singlet  $(cx)_4Fe$  structure calculated at the  $\square B97XD/DZP$  level.

## 5. Conclusion

The relatively high stability of the experimentally known homoleptic 1-norbornyl derivative  $(nor)_4Fe$  of iron in the unusual +4 oxidation state is a consequence of the high reaction barriers in the singlet and triplet potential surfaces. These potential surfaces are constrained by global dispersion attraction and the large steric demands of the norbornyl ligands as shown by their reduced density gradients (RDG) (Figure 13). Both dispersion effects and Coulombic interactions are essential in stabilizing the tetraalkylmetal compounds  $R_4M$ . These two effects are significantly

larger in the (nor)<sub>4</sub>M system than in the (cx)<sub>4</sub>M system, making the (nor)<sub>4</sub>M system too tight to distort.

The much more limited stability of the corresponding cyclohexyl derivative (cx)<sub>4</sub>Fe may result from the conical intersection between the singlet potential surface and the quintet spin potential surface arising from the weaker dispersion attraction and the reduced steric effect of the cyclohexyl ligands. In contrast, the high stability of the likewise experimentally known (cx)<sub>4</sub>M (M = Ru or Os)<sup>3</sup> structures results from the larger ligand field splitting ( $\Delta$ ) of the d-orbital energies for the second and third row transition metals ruthenium and osmium relative to that of the first row transition metal iron (Table 9). This leads to much larger singlet-triplet energy separations, thereby preventing the conical-intersection between the singlet potential energy surface and the high spin potential surfaces. This results in a significantly high energy barrier within the singlet potential surface for the (cx)<sub>4</sub>M  $\rightarrow$  (cx)<sub>2</sub>M + cx-cx reaction for the ruthenium and osmium derivatives relative to the iron derivative. The energies required for the alternative dissociation pathway (cx)<sub>4</sub>M  $\rightarrow$  (cx)<sub>3</sub>M + cx• (M = Ru or Os) are also much larger than that for (cx)<sub>4</sub>Fe compound (Tables 5 and 6).

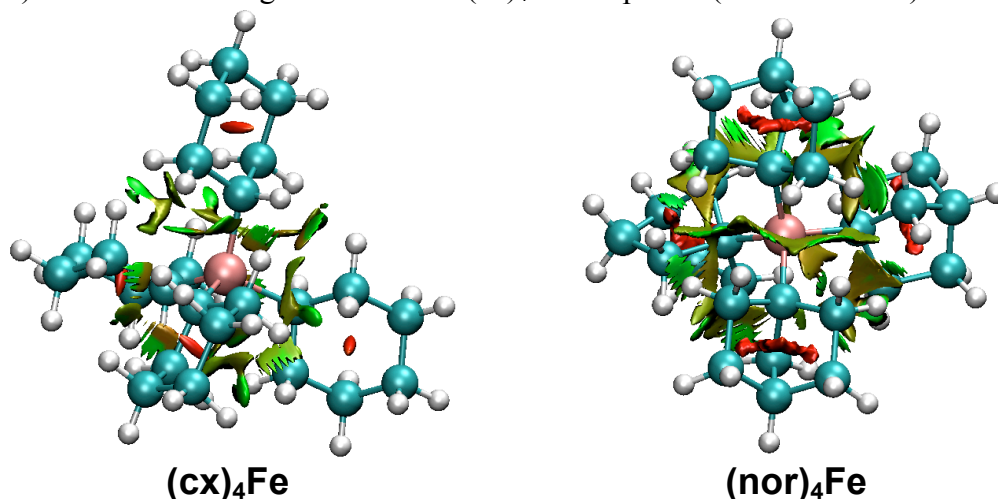


**Figure 13.** The reduced density gradient (RDG) for structures (cx)<sub>4</sub>Fe and (nor)<sub>4</sub>Fe.

### Acknowledgment

The research in Chengdu was supported by the Sichuan Provincial Foundation for Distinguished Young Leaders of Disciplines in Science and Technology of China (GrantNos.2019JDJQ0051 and 2019JDJQ0050), the Open Research Subject of the Key Laboratory of Advanced Computation in Xihua University (Grant No szjj2017-011 and szjj2017-012), the Young Scholarship Plan of Xihua University (Grant 0220170201), and the Chunhui Program of the Ministry of Education of China(Grant Z2017091). The research at the University of Georgia was supported by the U. S. National Science Foundation, Grant CHE-1661604.

The authors declare no competing financial interests.

## Supporting Information

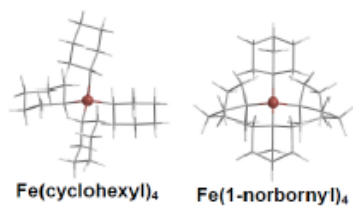
Tables S1 to S21: Atomic coordinates of the optimized structures for the lowest energy  $(cx)_nM$  complexes ( $n = 4, 3, 2$ ;  $M = Ti, V, Cr, Mn, Fe, Co, Ni, Cu$ ); Tables S22 to S42: Atomic coordinates of the optimized structures for the lowest energy  $(nor)_nM$  complexes ( $n = 4, 3, 2$ ;  $M = Ti, V, Cr, Mn, Fe, Co, Ni, Cu$ ); Complete Gaussian09 reference (Reference 23).

## Literature References

- (1) Lin, X.; Wu, W.; Mo, Y., Agostic interactions in early transition-metal complexes: roles of hyperconjugation, dispersion, and steric effect, *Chem. Eur. J.* **2019**, *25*, 6591–6599.
- (2) Schilter, D. High-valent iron gets homoleptic, *Nature Reviews Chemistry*, **2017**, *1*, 0036.
- (3) Lewis, R. A.; Smiles, D. E.; Darmon, J. M.; Stieber, S. C. E.; Wu, G.; Hayton, T. W. Reactivity and Mössbauer spectroscopic characterization of an Fe(IV) ketimide complex and reinvestigation of an Fe(IV) norbornyl complex. *Inorg. Chem.* **2013**, *52*, 8218–8227.
- (4) Dimitrov, V.; Linden, A. A pseudotetrahedral, high-oxidation state organonickel compound: synthesis and structure of bromotris(1-norbornyl)-nickel(IV). *Angew. Chem. Int. Ed.* **2003**, *42*, 2631-2633.
- (5) Bower, B. K.; Tennent, H. K. Transition metal bicyclo[2.2.1]hept-1-yls. *J. Am. Chem. Soc.* **1972**, *94*, 2512–2513.
- (6) Li, H.; Hu, Y.; Wan, D.; Zhang, Z.; Fan, Q.; King, R. B.; Schaefer, H. F. Dispersion effects in stabilizing organometallic compounds: The tetra-1-norbornyl derivatives of the first row transition metals as exceptional examples. *J. Phys. Chem. A.* **2019**, *123*, 9514–9519.
- (7) Casitas, A.; Rees, J. A.; Goddard, R.; Bill, E.; DeBeer, S.; Fürstner, A. Two exceptional homoleptic iron(IV) tetraalkyl complexes. *Angew. Chem. Int. Ed.* **2017**, *56*, 10108–10113.
- (8) Liptrot, D. J.; Guo, J.-D.; Nagase, S.; Power, P. P. Dispersion forces, disproportionation, and stable high-valent transition metal alkyls. *Angew. Chem. Int. Ed.* **2016**, *55*, 14766–14769.
- (9) Liptrot, D. J.; Power, P. P. London dispersion forces in sterically crowded inorganic and organometallic molecules, *Nature Reviews Chemistry* **2017**, *1*, 0004
- (10) Wagner, J. P.; Schreiner, P. R. London dispersion decisively contributes to the thermodynamic stability of bulky NHC-Coordinated main group compounds, *J. Chem. Theory Comput.* **2016**, *12*, 231–237.
- (11) Wagner, J. P.; Schreiner, P. R. London dispersion in molecular chemistry—reconsidering steric effects, *Angew. Chem. Int. Ed.* **2015**, *54*, 12274–12296.
- (12) Schreiner, P. R.; Chernish, L. V.; Gunchenko, P. A.; Tikhonchuk, E. Y.; Hausmann, H.; Serafin, M.; Schlecht, S.; Dahl, J. E. P.; Carlson, R. M. K.;

- Fokin, A. A. Overcoming lability of extremely long alkane carbon–carbon bonds through dispersion forces, *Nature* **2011**, *477*, 308-310
- (13) Wagner J. P.; Schreiner, P. R. London dispersion decisively contributes to the thermodynamic stability of bulky NHC-coordinated main group compounds, *J. Chem. Theory Comput.* **2016**, *12*, 231–237.
- (14) Israelachvilli, J. N. Intermolecular and surface forces; 3 ed., Academic Press: Waltham, USA, **2011**.
- (15) Li, H.; Feng, H.; Xie, Y.; Schaefer, H. F. The recently synthesized dimagnesiabutadiene and the analogous dimetalla-beryllium, -calcium, -strontium, and -barium compounds, *Chem. Eur. J.* **2016**, *22*, 15019-15026.
- (16) Stavropoulos, S.; Savage, P. D.; Tooze, R. P.; Wilkinson, G.; Hussein, B.; Motevalli, M.; Hursthouse, M. B. The synthesis and X-ray crystal structures of homoleptic tetrahedral aryls of osmium(IV) and of cyclohexyls of ruthenium(IV), osmium(IV), and chromium(IV), *J. Chem. Soc. Dalton*, **1987**, 557-561.
- (17) Israelachvilli, J. N. Intermolecular and surface forces; 3 ed., Academic Press: Waltham, USA, **2011**.
- (18) Perdew, J. P.; Wang, Y., Accurate and simple analytic representation of the electron gas correlation energy, *Phys. Rev. B*, **1992**, *45*, 13244-13249.
- (19) Perdew, J. P.; Burke, K.; Wang Y. Generalized gradient approximation for the exchange-correlation hole of a many-electron system. *Phys. Rev. B.* **1996**, *54*, 16533-16539.
- (20) Grimme, S. Density functional theory with London dispersion corrections. *Sires Comput. Mol. Sci.* **2011**, *1*, 211–228.
- (21) Dierksen, M.; Grimme, S. An efficient approach for the calculation of Franck-Condon integrals of large molecules. *J. Chem. Phys.* **2005**, *122*, 244101.
- (22) Chai, J. D.; Head-Gordon, M. Long-range corrected hybrid density functionals with damped atom-atom dispersion corrections. *Phys. Chem. Chem. Phys.* **2008**, *10*, 6615–6620.
- (23) Frisch, M. J.; *et al.* Gaussian 09, Revision A.02; Gaussian, Inc., Wallingford CT, 2009. See Supporting Information for further details.
- (24) Johnson, E. R.; Keinan, S.; Mori-Sánchez, P.; Contreras-García, J.; Cohen, A. J.; Yang, W.; Revealing noncovalent interactions, *J. Am. Chem. Soc.* **2010**, *132*, 18, 6498-6506.
- (25) Lu, T.; Chen F., Multiwfn: A multifunctional wavefunction analyzer, *J. Comput. Chem.*, **2012**, *33*, 580-592
- (26) Dunning, T. H., Jr. Gaussian basis functions for use in molecular calculations. I. Contraction of (9s5p) atomic basis sets for the first-row atoms. *J. Chem. Phys.* **1970**, *53*, 2823-2833.
- (27) Huzinaga, S. Gaussian-type functions for polyatomic systems. I. *J. Chem. Phys.* **1965**, *42*, 1293-1302.
- (28) Wachters, A. J. H. Gaussian basis set for molecular wavefunctions containing third-row atoms. *J. Chem. Phys.* **1970**, *52*, 1033-1036

- (29) Hood, D. M.; Pitzer, R. M.; Schaefer, H. F. Electronic structure of homoleptic transition metal hydrides:  $\text{TiH}_4$ ,  $\text{VH}_4$ ,  $\text{CrH}_4$ ,  $\text{MnH}_4$ ,  $\text{FeH}_4$ ,  $\text{CoH}_4$ , and  $\text{NiH}_4$ . *J. Chem. Phys.* **1979**, *71*, 705-712.
- (30) Neese, F.; Atanasov, M.; Bistoni, G.; Maganas, D.; Ye, S. Chemistry and quantum mechanics in 2019: Give us insight and numbers. *J. Am. Chem. Soc.* **2019**, *141*, 2814–2824.
- (31) Guo, Y.; Riplinger, C.; Becker, U.; Liakos, D. G.; Minenkov, Y.; Cavallo, L.; Neese, F. An improved linear scaling perturbative triples correction for the domain based local pair-natural orbital based singles and doubles coupled cluster method [DLPNO-CCSD(T)]. *J. Chem. Phys.* **2018**, *148*, 011101.
- (32) Neese, F. et.al, ORCA 4.1.2, An ab initio, DFT and semiempirical SCF-MO package, Max-Planck-Institut für Kohlenforschung.
- (33) Liu, S., Steric effect: A quantitative description from density functional theory, *J. Chem. Phys.* **2007**, *126*, 244103.
- (34) Jacobs, B.P.; Wolczanski, P. T.; Jiang, Q.; Cundari, T. R.; MacMillan, S. N. Rare examples of Fe(IV) alkyl-imide migratory insertions: impact of Fe–C covalency in  $(\text{Me}_2\text{IPr})\text{Fe}(=\text{NAd})\text{R}_2$  (R = neoPe, 1-nor), *J. Am. Chem. Soc.* **2017**, *139*, 12145–12148.
- (35) Cundari, T. R.; Jacobs, B. P. MacMillan, S. N.; Wolczanski, P. T. Dispersion forces play a role in  $(\text{Me}_2\text{IPr})\text{Fe}(=\text{NAd})\text{R}_2$  (Ad = adamantyl; R = <sup>neo</sup>Pe, 1-nor) insertions and Fe–R bond dissociation enthalpies (BDEs), *Dalton Trans.*, **2018**, *47*, 6025–6030.
- (36) Robbins, L. K. Lilly, C. P.; Sommer, R. D.; Ison, E. A. Effect of the ancillary ligand on the mechanism for CO migratory insertion in high-valent oxorhenium complexes, *Organometallics* **2016**, *35*, 3530-3537
- (37) Lambic, N. S.; Lilly, C. P.; Sommer, R. D.; Ison, E. A. Mechanism for the reaction of CO with oxorhenium hydrides: migratory insertion of CO into rhenium hydride and formyl bonds leads to migration from rhenium to the oxo ligand, *Organometallics* **2016**, *35*, 3060-3068.



TOC Figure